

Photocatalytic and adsorption property of ZnS–TiO₂/RGO ternary composites for methylene blue degradation

Adsorption Science & Technology

2019, Vol. 37(9–10) 764–776

© The Author(s) 2018

DOI: 10.1177/0263617418810932

journals.sagepub.com/home/adt

**YL Qin, WW Zhao and Z Sun**

School of Science, Shenyang Ligong University, Shenyang, China;
Shenyang National Laboratory for Materials Science, Institute of Metal
Research, Chinese Academy of Sciences, Shenyang, China

XY Liu

School of Science, Shenyang Ligong University, Shenyang, China

GL Shi

Zolix Instruments Co., Ltd., Beijing, China

ZY Liu, DR Ni and ZY Ma

Shenyang National Laboratory for Materials Science, Institute of Metal
Research, Chinese Academy of Sciences, Shenyang, China

Abstract

The visible light-driven ZnS–TiO₂/RGO nanocomposites, with good visible light-driven photocatalytic activity, utilizing graphene oxide as precursor, were successfully synthesized via a facile solvothermal thermal method with graphene oxide as precursor. Ti⁴⁺ ions were derived from titanium dioxide powder (TiO₂, P25) and tetrabutyl titanate. S²⁻ ions and Zn²⁺ ions were provided by sodium sulfide and zinc acetate, respectively. The photocatalytic and absorbance activity of the nanocomposites was investigated through the photocatalytic degradation of methylene blue in aqueous solution. The results showed that the ZnS–TiO₂/RGO nanocomposite prepared by tetrabutyl titanate exhibited better photocatalytic and adsorbance activity for methylene blue under visible light irradiation and its photocatalytic efficiency reached 90% in 60-min light irradiation, almost 1.5 times that of the synthesized ZnS–TiO₂/RGO by P25, which was attributed to

Corresponding author:

DR Ni, Shenyang National Laboratory for Materials Science, Institute of Metal Research, Chinese Academy of Sciences, 72 Wenhua Road, Shenyang 110016, China.

Email: drni@imr.ac.cn



Creative Commons CC BY: This article is distributed under the terms of the Creative Commons Attribution 4.0 License (<http://www.creativecommons.org/licenses/by/4.0/>) which permits any use, reproduction and distribution of the work without further permission provided the original work is attributed as specified on the SAGE and Open Access pages (<https://us.sagepub.com/en-us/nam/open-access-at-sage>).

a cooperative reaction because of an increase of photo-absorption effect of graphene sheets and photocatalytic effect of ZnS nanoparticles. The adsorbance activity for ZnS–TiO₂/RGO–tetra-butyl titanate) reached 48%, which was almost 1.7 times higher than that of ZnS–TiO₂/RGO-P25 and almost 3.7 times higher than that of ZnS/RGO.

Keywords

Solvothermal method, TiO₂, nanocomposites, graphene, photocatalytic degradation, adsorbance

Submission date: 3 September 2017; Acceptance date: 24 September 2018

Introduction

At present, environmental problems caused by the undegraded organic pollutions and the harmful compounds such as pesticides and dyes have negative effect on the human being survival and development (Kim and Herrera, 2010; Liu et al., 2016; Sookhakian et al., 2014; Zeng et al., 2014; Zhang et al., 2016). It is difficult to solve these problems by the traditional environment technology. Much more attentions have been paid to the photocatalytic degradation and complete mineralization of undegraded organic compounds in water, soil, and air using the semiconductor photocatalyst method (Hamadianian et al., 2010). Since Fujishima and Honda firstly reported the use of titanium dioxide (TiO₂) as photocatalyst to decompose water-producing hydrogen (Fujishima and Honda, 1972; Fujishima et al., 2008), various semiconductors have been developed for photocatalytic degradation of pollutants. Photocatalytic activity of semiconductors depends mainly on the oxidation–reduction potentials of the valence band and the conduction band. The semiconductors with oxidation–reduction potential of the conduction band are more negative, while oxidation–reduction potential of the valence band is more positive own strong oxidation and reduction ability of photogenerated electrons and holes, thus the efficiency of photocatalytic degradation of organic contaminants is greatly improved.

Presently, TiO₂ is expected to be one of the most promising materials due to its chemical stability, nontoxicity, low price, and superior photoactivity (Azimi et al., 2016; Hu et al., 2005; Minella et al., 2017; Yanagida et al., 1986). However, in practical application, TiO₂ is with two main drawbacks: (1) the light absorption of TiO₂ with relatively larger band gap (~3.2 eV) is limited to shorter wavelength in ultraviolet light which is shorter than 10% of the solar spectrum. (2) Photogenerated electron-hole pairs are easier to be recomposed, reducing the photoelectric conversion efficiency, and then decreasing the photocatalytic efficiency (Khanna and Shetty, 2014; Xiang et al., 2012; Wang et al., 2017). In order to suppress carrier recombination and obtain the visible light photocatalyst materials, a great deal of efforts have been paid to dope with nonmetal elements C, N, S etc. (Cao et al., 2013; Malato et al., 2007) and developed new photocatalyst materials with the absorption spectrum in visible range (400–800 nm) (Asahi et al., 2001).

The development of semiconductor composites with nanometer sizes is one of the most effective approaches to effectively utilize the visible light. For example, the semiconductor composites including (MS/TiO₂) (M = Pb, Zn, Cd) exhibited fine optical properties (absorption and photoluminescence (PL)) compared with the normal ones because of the quantum confinement effects (Su et al., 2001). Steng et al. (2008) reported the synthesis of ZnS/TiO₂

nanocomposites for the photocatalytic decomposition of Orange II dye. The nanocomposites showed efficient visible-light photocatalytic activity, which is higher than that of a commercially available TiO₂ (Degussa P25), pure anatase TiO₂, or cubic ZnS nanoparticles. Franco et al. (2009) prepared nanocomposites of (ZnS/TiO₂) with different ZnS: TiO₂ ratios using a chemical deposition method. The presence of small ZnS percentages on the nanocomposite surface (0.5% and 0.2%) promoted an increase on the catalyst photoactivity compared with the original TiO₂. Yu et al. (2006) fabricated ZnS/TiO₂ nanocomposites exhibiting enhanced visible-light photocatalytic activity for the aqueous parathion–methyl degradation, which is attributed to the formation of the preassociated complex and the synergetic effect resulting from the combination of the cubic ZnS and anatase TiO₂. However, how to further improve the photocatalytic property of this kind of composites is still a great challenge.

Graphene, a two-dimensional single layer of sp² hybridized carbon atoms with large specific surface area, performs excellent thermal conductivities, high charge carrier mobility, and remarkable mechanical strength and flexibility. It has been a potential candidate to facilitate the adsorption capability and photocatalytic activity of TiO₂ and ZnS due to their effective electron transfer and interaction effects (Chakraborty et al., 2016; Qin et al., 2014, 2017b). Photocatalysts with graphene composites have been carried out by using various methods. Zhang et al. (2010) obtained a chemically bonded TiO₂ (P25)–graphene nanocomposite photocatalyst with graphene oxide (GO) and P25, using a facile one-step hydrothermal method. Park et al. (2014) reported that ZnS combined graphene/TiO₂ (ZGT) composites were prepared by a sol–gel method. Wang et al. (2012) compounded the single crystal TiO₂ nanoparticles exposing high energy with graphene by one-step solvothermal method, simultaneously, GO was reduced in the formation of RGO. The prepared composite materials showed enhancing photocatalytic degradation property compared with pure TiO₂.

According to our previous work, the nanocomposite prepared with sodium sulfide as the S²⁻ source exhibited much better photocatalytic degradation efficiency than that with thiourea (Qin et al., 2017a). Herein, we proposed a facile and reproducible solvothermal route to obtain ZnS–TiO₂/RGO (ZTR) nanocomposites for the first time. In the present study, graphene was added into ZnS–TiO₂ nanophotocatalyst in order to improve their photocatalytic activity. The effect of different Ti⁴⁺ ions sources on structural, morphological, optical, and photocatalytic properties of the nanocomposites has been figured out. Methylene blue (MB) was selected as a typical dye to evaluate the photocatalytic activity of the nanocomposites under visible light.

Experimental

Materials

Zinc acetate (Zn (Ac)₂·2H₂O), sodium sulfide (Na₂S·9H₂O), tetrabutyl titanate (TBOT), MB, ethylene glycol, and absolute ethanol were obtained from Chinese Medicine Group Chemical Reagent Co. Ltd. GO aqueous solution was purchased from Shanxi Coal Research Institute of Chinese Academy of Sciences, and TiO₂ powder (P25) was obtained from Degussa Specialty Chemicals Co. Ltd. All of these chemical reagents were of analytical grade and used as received without any further purification, and deionized water was used to wash samples in all experiments.

Preparation of ZTR photocatalysts using P25 (ZTR–P25)

At first, 0.5 mmol of $\text{Zn}(\text{Ac})_2 \cdot 2\text{H}_2\text{O}$ was dissolved in 20 mL ethylene glycol ($(\text{CH}_2\text{OH})_2$) and then 10 mL GO aqueous solution (2mg/L) was added into the solution, forming the light brown solution after sonication for 0.5 h. Next, 0.5 mmol $\text{Na}_2\text{S} \cdot 9\text{H}_2\text{O}$ and 0.5 mmol TiO_2 powder were dissolved in 20 mL ethylene glycol respectively, following ultrasonic vibration for 0.5 h, and then added into the above-mentioned light brown solution. The mixture was treated by ultrasonic vibration and magnetic stirring for 1 h and transferred into 100 mL Teflon-lined stainless steel autoclave and heated to 180°C for 10 h. The reaction mixture was cooled down to the room temperature and the precipitate was filtered, washed with deionized water and ethanol for several times, and dried in a vacuum oven at 60°C .

Preparation of ZTR photocatalysts using TBOT (ZTR–TBOT)

In a typical reaction procedure, 0.5 mmol $\text{Zn}(\text{Ac})_2 \cdot 2\text{H}_2\text{O}$ was dissolved in 20 mL absolute ethanol and 20 mg GO powder was added to the solution. The mixture's color becomes light brown after sonication for 0.5 h. Then, 0.5 mmol $\text{Na}_2\text{S} \cdot 9\text{H}_2\text{O}$ was dissolved in 20 mL absolute ethanol with sonication for 0.5 h. The above two systems were then mixed together and 3 mL TBOT was added into the mixture under the condition of agitation, following ultrasonic vibration and magnetic stirring for 1 h. Then the mixture was transferred into an autoclave. The sealed autoclave was kept at 180°C for 10 h. The obtained precipitates were filtered and washed several times with deionized water and absolute ethanol, then they were dried at 60°C .

Characterization

X-ray power diffraction (XRD) patterns of samples were recorded on D/max 2400 X-ray diffractometer (Neo Confucianism, Japanese) using CuK α radiation source with wavelength of 1.54056 Å to obtain the crystal phases of the composite photocatalysts. Transmission electron microscopy (TEM) images were taken with a F20 microscope (FEI, America) operating at 200 kV, by depositing a drop of sample dispersion onto 300 mesh Cu grids coated with a carbon layer. Raman and PL spectra of samples were taken on a Finder Vista spectrometer (Zolix, China) to observe the chemical structures of the materials. The UV–vis absorption spectrum was recorded with a homemade UV–vis spectrometer.

Photocatalytic tests

The photocatalytic performances of all nanocomposites were evaluated by the degradation curves in a 20 mg/L MB aqueous solution under visible light for different interval times. The experiment of photocatalytic reaction was carried out using a 500 w xenon lamp ($\lambda > 420\text{ nm}$). In each experiment, the photochemical reactor contained 20 mg ZTR catalysts and 50 mL of 20 mg/L MB aqueous solution. Before starting the illumination, the reaction mixture was stirred for 30 min in dark to reach the adsorption–desorption equilibrium between the MB and the photocatalyst. Three milliliters aliquots were withdrawn from the suspension and then centrifugally separated to essentially remove all the catalyst after a given time interval of irradiation. The concentration of the remnant dye was spectrophotometrically monitored by recording the variation of the absorption band maximum in the UV–vis spectrum of MB (663 nm).

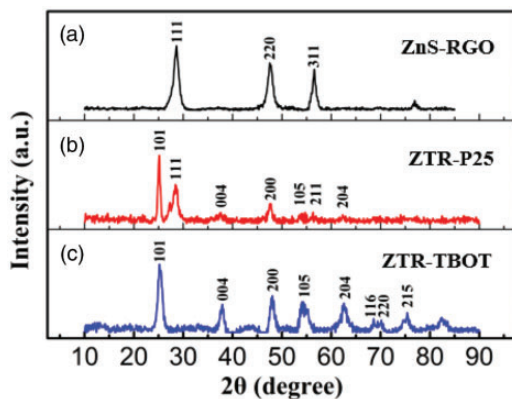


Figure 1. XRD patterns of ZnS/RGO composites and ZTR ternary composites.

Results and discussion

Characteristics of nanocomposites

Figure 1 shows the XRD patterns of both ZnS/RGO and ZTR nanocomposites. It can be seen that ZnS (Figure 1(a)) reveals three major peaks at $2\theta = 28.97^\circ$, 48.3° , and 57.1° corresponding to the crystal planes of (111), (220), and (311), respectively, which makes a good agreement with the face-centered cubic phase of ZnS (JCPDS card No. 05–0566). That is, (101), (004), (200), (105), (211), (204), and (116) crystal planes are originated from the anatase TiO_2 phase (JCPDS file No. 21–1272). XRD spectrum of the ZTR composites prepared using P25 (Figure 1(b)) shows the characteristic diffraction peaks of ZnS, because of the absorption of Zn^{2+} ions on the surface of GO and the initial formation of ZnS micronucleus on the surface of RGO; however, TiO_2 powder hardly exists in the preparation process with the state of Ti^{4+} ions due to its indissolubility which leads to a small amount of TiO_2 attaching to the RGO surface. While the XRD spectra of the composites prepared using TBOT (Figure 1(c)), clearly shows the diffraction peaks of anatase TiO_2 phase. The diffraction peaks of ZnS cannot be observed. These experimental results indicate that TiO_2 nanoparticles can be loaded on the RGO surface through hydrogen bonding, and the negative charge characteristics of GO powder dissolved in ethanol is weakened or even disappeared, resulting in a few ZnS particles adhered to the RGO surface.

The morphologies of these two nanocomposites were characterized by TEM, as shown in Figure 2. Figure 2(a) shows that the graphene is a homogeneous and smooth sheets. While, Figure 2(b) presents that only TiO_2 nanoparticles locate on the graphene sheet and these particles are heavily aggregated in the composites by TBOT because GO powder is not completely dissolved and dispersed in absolute ethanol that results in few ZnS particles adhering to the surface of GO. high resolution transmission electron microscope (HRTEM) images of these two nanocomposites are suggested as shown in Figure 2(c) and (d). The lattice distances of 0.308 nm and 0.352 nm correspond to the interplanar distance of the (111) plane of cubic ZnS phase and the (101) plane of anatase TiO_2 phase, respectively.

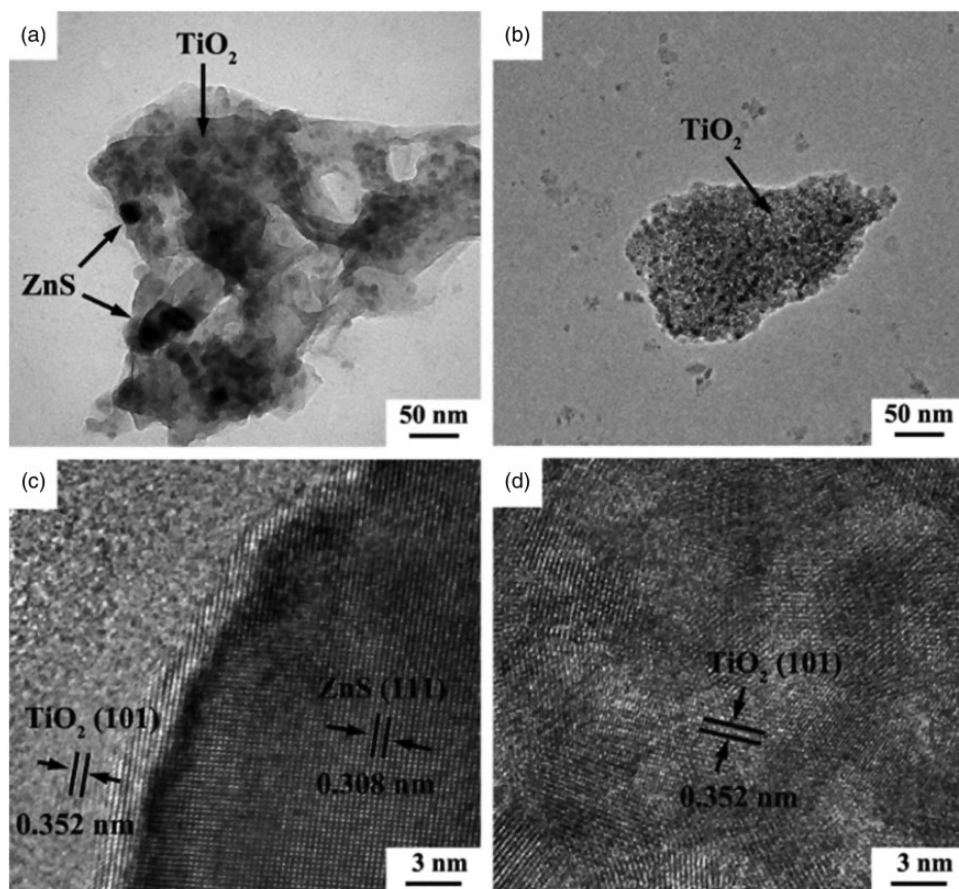


Figure 2. TEM and HRTEM images of ZTR ternary composites prepared by P25 (a, c) and TBOT (b, d).

Figure 3 displays the Raman spectra of the GO, graphite, and ZTR nanocomposites. The two typical peaks of GO can be found at 1345 cm^{-1} and 1589 cm^{-1} , which correspond to the D bands assigned to the E_{2g} phonon mode of sp^2 -bonded carbon atoms and G bands are attributed to the breathing mode of A_{1g} symmetry from phonon interaction near the K zone boundary (Shen et al., 2006). With the reduction of GO, the D bands of ZTR composites shift to lower wave numbers around 1330 cm^{-1} , and the G bands change to higher wave numbers of 1594 cm^{-1} compared to GO. However, the movement of D and G bands indicates that there is an interaction between semiconductor nanoparticles and graphene. In addition, the disorder degree of composites synthesized by P25 and TBOT can be respectively estimated from the intensity ratio of the D to G bands (I_D/I_G). As shown in Figure 3 (c), the ratio of the ZTR-P25 composite is higher than that of the ZTR-TBOT composite.

Photocatalytic properties of nanocomposites

As shown in Figure 4, PL spectra of the as-prepared samples were investigated with the excitation wavelength of 325 nm . It was reported that the photocatalytic degradation

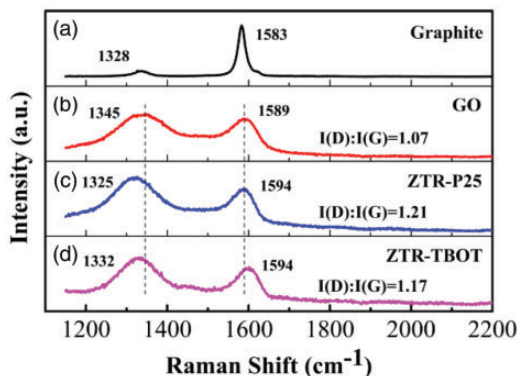


Figure 3. Raman patterns of Graphite (a), GO (b), ZTR-P25 (c), and ZTR-TBOT (d) ternary composites.

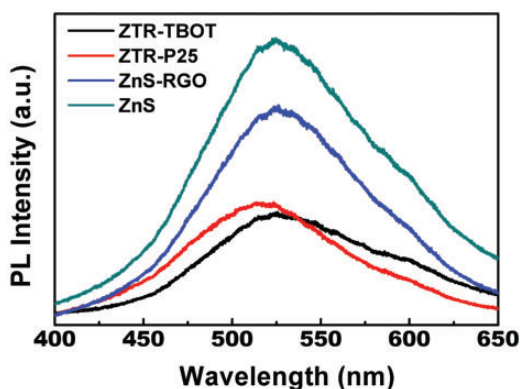


Figure 4. PL spectra for ZTR nanocomposites compared to ZnS and ZnS-RGO.

efficiency of materials was related to the efficiency of charge carriers trapping, migration and transfer of the photogenerated electrons and holes (Pant et al., 2016). The PL spectra of ZnS exhibits a sharp green emission peak, which is ascribed to self-activated defect center relating to the presence of Zn vacancies in ZnS/RGO nanoparticles. In Figure 4, it is noticeable that the luminescence efficiency of the ZTR-P25, ZTR-TBOT and ZnS/RGO are all lower than that of bare ZnS. In particular, ZTR-TBOT composite performs the lowest PL intensity, which verifies that the recombination of electron-hole pair is effectively reduced along with the prolongation of lifetime of photogenerated carriers due to the synergistic effect of ZnS and TiO₂ on RGO (Pant et al., 2016).

As shown in Figure 5, the intensity of the absorption peak of MB at 663 nm decreases with the increase of irradiation time due to the photocatalytic activity between ZTR-P25 and ZTR-TBOT, which indicates that the MB molecules are degraded by the catalysis. Furthermore, we compared the photocatalytic and adsorption performance of ZnS-RGO and ZnS with ZTR on MB degradation (Figure 6). It demonstrates that the ZTR nanocomposites have superior photocatalytic activity, particularly prepared by TBOT.

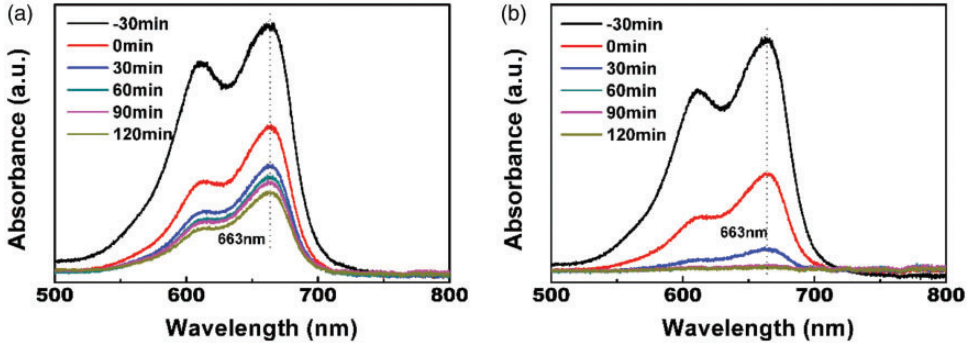


Figure 5. Absorption spectra of MB aqueous solution degraded by ZTR nanocomposites: (a) ZTR–P25 and (b) ZTR–TBOT.

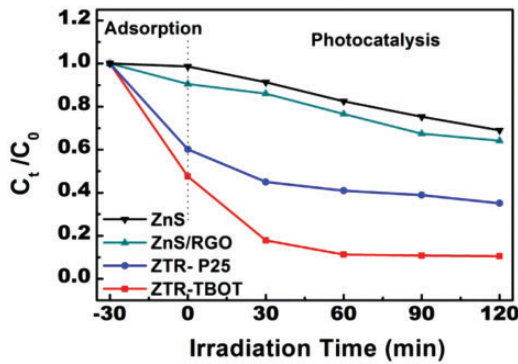


Figure 6. Photocatalytic degradation rates of MB for all catalysts.

After 120 min of light irradiation, the degradation efficiency of bare ZnS and ZnS/RGO catalysts is about 30% and 38% for MB, whereas the nanocomposites show increased degradation efficiency by about 65% for ZTR–P25 and 90% for ZTR–TBOT. The reason is that the surface of ZTR is larger than that of ZnS and ZnS/RGO. On the other hand, the strong π - π conjugated connection between the benzene rings of pollution and the surface of RGO can also enhance the pollutants adsorption (Nawaz et al., 2017). The adsorbance activity for ZTR–TBOT reached 48%, which is almost 1.7 times higher than that of ZTR–P25 and almost 3.7 times higher than that of ZnS/RGO.

The photocatalytic degradation process accompanied with pseudo first-order kinetics and the rate constant can be calculated using well-known first-order rate law equation as follows (Soltani and Entezari, 2013)

$$-\ln(C_t/C_0) = kt \tag{1}$$

where C_t and C_0 are the concentration at irradiation time t and the initial concentration, respectively; k is a constant which stands for the photocatalytic degradation rate.

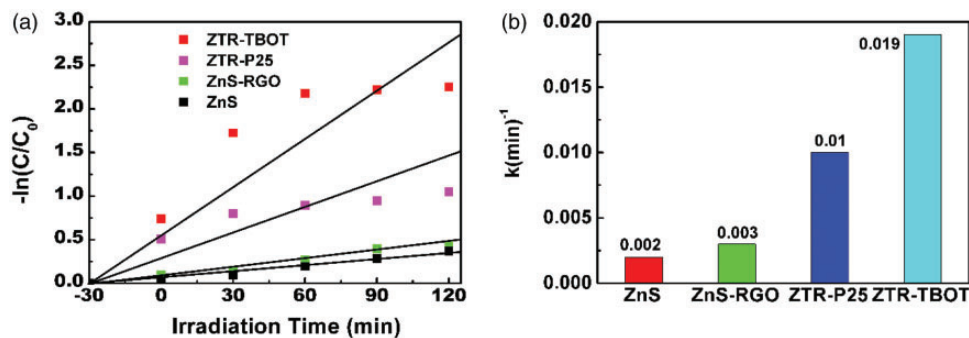


Figure 7. Photocatalytic rate constant curves and columns of MB for various catalysts.

Table 1. Comparative performance of the ZnS–TiO₂/RGO (ZTR)-tetrabutyl titanate (TBOT) composite with reported photocatalyst for methylene blue (MB) degradation with reaction parameters.

Sample	Catalyst content	MB concentration	Light source	PH	Photocatalytic degradation rate, K , min ⁻¹	Ref.
ZTR–TBOT	20 mg	20 mg/L	500 W xenon lamp	7	0.019	This paper
TiO ₂ –GO	50 mg	20 mg/L	175 W high pressure mercury lamp	7	0.0138	Liu et al. (2016)
TiO ₂ –GO	0.5 g dm ⁻³	4 × 10 ⁻⁵ M	3 TLK 40 W/05 (UV–vis) fluorescent lamps	3	0.014–0.040	Minella et al. (2017)
TiO ₂ –GO	0.5 g dm ⁻³	4 × 10 ⁻⁵ M	Vis only	3	0.0129–0.026	Minella et al. (2017)

The photodegradation linear plots of $-\ln(C_t/C_0)$ vs. t (time) for MB are shown in Figure 7 (a). Figure 7(b) obviously displays that constant k of ZTR–TBOT is the highest, i.e. about 1.9 times of ZTR–P25 and almost 6.3 and 9.5 times of ZnS/RGO and pure ZnS, respectively. This shows that through combination of semiconductor with the loading big surface material of graphene sheets, the ZTR–TBOT has prominent synergistic effect among the individual constituents of the catalyst, including RGO served as an electron capture device to boost the transfer of the photoexcited charges, and TiO₂ nanoparticles also effectively improve the solar-light absorption by introducing ZnS (Tian et al., 2016). Table 1 shows a comparative performance of the ZTR–TBOT composite with reported photocatalyst for MB degradation with reaction parameters. Because of the different testing conditions, it is difficult to point out which photocatalyst has better photodegradation performance, but on the whole, the ZTR–TBOT composite has good photodegradation performance.

Based on the above analysis, a potential mechanism for photocatalytic degradation of MB over ternary ZTR nanocomposites under light irradiation is proposed in Figure 8, and the detailed process is expressed by the equations (2) to (6). The formation of electron-hole pairs at the semiconductor surface upon light irradiation (energy higher than that of the band energy of semiconductor) will lead to a series of chain reaction mediated via OH· and

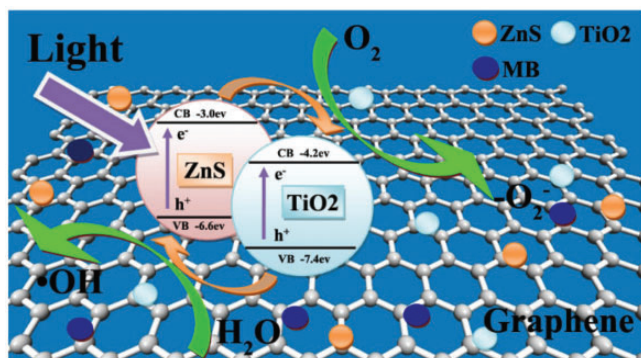
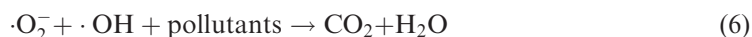
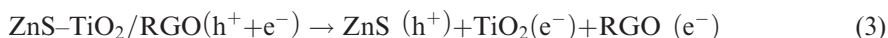
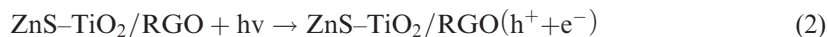


Figure 8. Mechanism for photodegradation of MB by ZTR nanocomposites under visible light irradiation.

$O_2\cdot$ generation which further results in the photodegradation of dye or pollutants (Kashinath et al., 2017; Thangavel et al., 2016). When the ZTR photocatalyst is irradiated under visible light, the electrons from the valence band are excited into the conduction band of ZnS, leaving the holes in the valence band, and then are transferred to the conduction band of TiO_2 . Since the extremely high electron mobility of graphene, the electrons transferred from TiO_2 to graphene are captured by O_2 to produce $O_2^{\cdot-}$. Additionally, photo-generated holes will be left in the valence band of ZnS–graphene, migrating to the surface and oxidizing hydroxyl to produce $\cdot OH$, which makes a major contribution to the MB oxidation. The specific process is as follows (Park et al., 2014)



Conclusion

In this work, photocatalytic composites of ZTR prepared by using TiO_2 (P25) powder and TBOT as precursors respectively were successfully obtained in a simple solvothermal method to improve the photocatalysis effectively. GO was reduced into RGO during this synthesis process. The photocatalytic and adsorption results illustrate that (i) The tricomponent composites showed high quantum efficiency across the UV–vis light spectrum compared to both the single and bicomponent constructions, highlighting a synergetic charge separation and efficient charge transport channel; (ii) the ZTR–TBOT with the highest rate constant k exhibited superior photocatalytic activity and stability due to the increase of

electron conduction and electron-hole separation ability; (iii) RGO increases the specific surface areas of the composites for more adsorbed MB and facilitates the charge transportation and separation.

Author contributions

YLQ and WWZ contributed equally to this work, and they conceived the idea and designed the experiments. WWZ, ZS, GLS, ZYL, and XYL performed the experiments. YLQ and WWZ wrote the paper under the supervision of DRN and ZYM. All authors participated in the data analysis and discussion.

Declaration of Conflicting Interests

The author(s) declared no potential conflicts of interest with respect to the research, authorship, and/or publication of this article.

Funding

The author(s) disclosed receipt of the following financial support for the research, authorship, and/or publication of this article: The authors gratefully acknowledge the support of the program of Liaoning Education Department Nos. LG201605, Key Laboratory Open Fund of Shenyang Li gong University Nos. 4801004yb61-d and 4771004kfs49, and the National Basic Research Program of China under Grant Nos. 2011CB932603 and the CAS/SAFEA International Partnership Program for Creative Research Teams.

References

- Asahi R, Morilawa T, Ohwaki T, et al. (2001) Visible-light photocatalysis in nitrogen-doped titanium oxides. *Science* 293: 269–271.
- Azimi HR, Ghoranneviss M, Elahi SM, et al. (2016) Photovoltaic and UV detector applications of ZnS/rGO nanocomposites synthesized by a green method. *Ceramics International* 42: 14094–14099.
- Cao SY, Chen CS, Ning XT, et al. (2013) Preparation and photocatalytic property of graphene/TiO₂ composite powder. *Integrated Ferroelectrics* 145: 40–45.
- Chakraborty K, Chakrabarty S, Das P, et al. (2016) UV-assisted synthesis of reduced graphene oxide zinc sulfide composite with enhanced photocatalytic activity. *Materials Science and Engineering. B* 204: 8–14.
- Franco A, Neves MC, Carrott MMLR, et al. (2009) Photocatalytic decolorization of methylene blue in the presence of TiO₂/ZnS nanocomposites. *Journal of Hazardous Materials* 161: 545–550.
- Fujishima A and Honda K (1972) Electrochemical photolysis of water at a semiconductor electrode. *Nature* 238: 37–38.
- Fujishima A, Zhang XT and Tryk DA (2008) TiO₂ photocatalysis and related surface phenomena. *Surface Science Reports* 63: 515–582.
- Hamadani M, Reisi-Vanani A and Majedi A (2010) Synthesis, characterization and effect of calcination temperature on phase transformation and photocatalytic activity of Cu,S-codoped TiO₂ nanoparticles. *Applied Surface Science* 256: 1837–1844.
- Hu JS, Ren LL, Guo YG, et al. (2005) Mass production and high photocatalytic activity of ZnS nanoporous nanoparticles. *Angewandte Chemie International Edition* 44: 1269–1273.
- Kashinath L, Namratha K and Byrappa K (2017) Sol-gel assisted hydrothermal synthesis and characterization of hybrid ZnS-RGO nanocomposite for efficient photodegradation of dyes. *Journal of Alloys and Compounds* 695: 799–809.

- Khanna A and Shetty VK (2014) Solar light induced photocatalytic degradation of reactive blue 220 (RB-220) dye with highly efficient Ag@TiO₂ core-shell nanoparticles: A comparison with UV photocatalysis. *Solar Energy* 99: 67–76.
- Kim EJ and Herrera JE (2010) Characteristics of lead corrosion scales formed during drinking water distribution and their potential influence on the release of lead and other contaminants. *Environmental Science & Technology* 44: 6054–6061.
- Liu XW, Shen LY and Hu YH (2016) Preparation of TiO₂-graphene composite by a two-step solvothermal method and its adsorption-photocatalysis property. *Water, Air, & Soil Pollution* 227: 141.
- Malato S, Blanco J, Alarcon DC, et al. (2007) Photocatalytic decontamination and disinfection of water with solar collectors. *Catalysis Today* 122: 137–149.
- Minella M, Sordello F and Minero C (2017) Photocatalytic process in TiO₂/graphene hybrid materials. Evidence of charge separation by electron transfer from reduced graphene oxide to TiO₂. *Catalysis Today* 281: 29–37.
- Nawaz M, Miran W, Jang J, et al. (2017) One-step hydrothermal synthesis of porous 3D reduced graphene oxide/TiO₂ aerogel for carbamazepine photodegradation in aqueous solution. *Applied Catalysis B: Environmental* 203: 85–95.
- Pant B, Park M, Park SJ, et al. (2016) One-pot synthesis of CdS sensitized TiO₂ decorated reduced graphene oxide nanosheets for the hydrolysis of ammonia-borane and the effective removal of organic pollutant from water. *Ceramics International* 42: 15247–15252.
- Pant B, Saud PS, Park M, et al. (2016) General one-pot strategy to prepare Ag–TiO₂ decorated reduced graphene oxide nanocomposites for chemical and biological disinfectant. *Journal of Alloys and Compounds* 671: 51–59.
- Park CY, Choi JG, Ghosh T, et al. (2014) Preparation of ZnS-graphene/TiO₂ composites designed for their high photonic effect and photocatalytic activity under visible light. *Fullerenes Nanotubes and Carbon Nanostructures* 22: 630–642.
- Qin HY, Xu Y, Kim J, et al. (2014) The effect of structure on the photoactivity of a graphene/TiO₂ composite. *Materials Science and Engineering B* 184: 72–79.
- Qin YL, Sun Z, Zhao WW, et al. (2017a) Effect of S²⁻ donors on synthesizing and photocatalytic degrading properties of ZnS/RGO nanocomposite. *Applied Physics A* 123: 355.
- Qin YL, Sun Z, Zhao WW, et al. (2017b) Improved photocatalytic properties of ZnS/RGO nanocomposites prepared with GO solution in degrading methyl orange. *Nano-Structures Nano-Objects* 10: 176–181.
- Shen GZ, Bando Y and Golberg D (2006) Self-assembled three-dimensional structures of single-crystalline ZnS submicrotubes formed by coalescence of ZnS nanowires. *Applied Physics Letters* 88: 123107.
- Soltani T and Entezari MH (2013) Solar photocatalytic degradation of RB5 by ferrite bismuth nanoparticles synthesized via ultrasound. *Ultrasonics Sonochemistry* 20: 1245–1253.
- Sookhikian M, Amin YM, Baradaran S, et al. (2014) A layer-by-layer assembled graphene/zinc sulfide/polypyrrole thin-film electrode via electrophoretic deposition for solar cells. *Thin Solid Films* 552: 204–211.
- Steng V, Bakardjieva S, Murafa N, et al. (2008) Visible-light photocatalytic activity of TiO₂/ZnS nanocomposites prepared by homogeneous hydrolysis. *Microporous and Mesoporous Materials* 110: 370–378.
- Su HL, Xie Y, Gao P, et al. (2001) Synthesis of MS/TiO₂ (M = Pb, Zn, Cd) nanocomposites through a mild sol-gel process. *Journal of Materials Chemistry* 11: 684–686.
- Thangavel S, Krishnamoorthy K, Kim SJ, et al. (2016) Designing ZnS decorated reduced graphene-oxide nanohybrid via microwave route and their application in photocatalysis. *Journal of Alloys and Compounds* 683: 456–462.

- Tian HW, Wan CX, Zheng WT, et al. (2016) Construction of a ternary hybrid of CdS nanoparticles loaded on mesoporous-TiO₂/RGO for the enhancement of photocatalytic activity. *RSC Advances* 6: 84722–84729.
- Wang W, Huang XG, Lai M, et al. (2017) RGO/TiO₂ nanosheets immobilized on magnetically actuated artificial cilia film: a new mode for efficient photocatalytic reaction. *RSC Advances* 7: 10517–10523.
- Wang WS, Wang DH, Qu WG, et al. (2012) Large ultrathin anatase TiO₂ nanosheets with exposed {001} facets on graphene for enhanced visible light photocatalytic activity. *The Journal of Physical Chemistry C* 116: 19893–19901.
- Xiang QJ, Yu JG and Jaroniec M (2012) Graphene-based semiconductor photocatalysts. *Chemical Society Reviews* 41: 782–796.
- Yanagida S, Mizumoto K and Pac C (1986) Semiconductor photocatalysis.6. cis-trans photoisomerization of simple alkenes induced by trapped holes at surface-states. *Journal of the American Chemical Society* 108: 647–654.
- Yu XD, Wu QY, Jiang SC, et al. (2006) Nanoscale ZnS/TiO₂ composites: Preparation, characterization, and visible-light photocatalytic activity. *Materials Characterization* 57: 333–341.
- Zeng B, Chen XH, Chen CS, et al. (2014) Reduced graphene oxides loaded-ZnS/CuS heteronanostructures as high-activity visible-light-driven photocatalysts. *Journal of Alloys and Compounds* 582: 774–779.
- Zhang H, Lv XJ, Li YM, et al. (2010) P25-graphene composite as a high performance photocatalyst. *ACS Nano* 4: 380–386.
- Zhang Y, Shi BY, Zhao YY, et al. (2016) Deposition behavior of residual aluminum in drinking water distribution system: Effect of aluminum speciation. *Environmental Science & Technology* 42: 142–151.